

HOSTED BY



Contents lists available at ScienceDirect

Journal of King Saud University – Science

journal homepage: www.sciencedirect.com

Original article

The highly efficient green synthesis of nanostructured ZnFe₂O₄ photocatalysts by using *Ziziphus mauritiana* and *Salvadora persica* extracts for the photocatalytic degradation of crystal violet in sunlight



Hossein Bayahia

Chemistry Department, Faculty of Science, Albaha University, Albaha, Saudi Arabia

ARTICLE INFO

Article history:

Received 5 November 2022

Revised 26 January 2023

Accepted 30 January 2023

Available online 08 February 2023

Keywords:

ZnFe₂O₄

Extracts

Degradation

Crystal violet

Sunlight

ABSTRACT

The current study is aimed to investigate the photocatalytic degradation of crystal violet dyes solution in the presence of modified ZnFe₂O₄ photocatalysts by *Ziziphus mauritiana* and *Salvadora persica* extracts in sunlight. Regardless of the extracts used, the modified ZnFe₂O₄ catalysts demonstrated excellent photocatalytic degradation. However, the catalysts modified using *Salvadora persica* extract achieved superior photocatalytic degradation of crystal violet dye. ZnFe₂O₄ with *Salvadora persica* yielded smaller particles with a larger surface area, smaller band gap energy and a better distribution of differently sized particles than by using *Ziziphus mauritiana*. This photocatalyst also demonstrated stability, being able to be reused at least five times with minimal loss of catalytic ability, falling from 91% at the first iteration to 85% by the fifth reuse. These materials were prepared easily using an environmentally friendly method.

© 2023 The Author(s). Published by Elsevier B.V. on behalf of King Saud University. This is an open access article under the CC BY-NC-ND license (<http://creativecommons.org/licenses/by-nc-nd/4.0/>).

1. Introduction

Today, the water contamination and the energy crisis are the major concerns and they lie in the remarkable processes of photocatalysis (Mehtab et al., 2022a). The methods of synthesis of nanoparticles along with the photocatalytic degradation strategy have been broadly used to eliminate of harmful industrial pollutants and colour in the wastewater (Haseena et al., 2022) by elimination of recombination of electron and hole to their utilization in the photocatalytic degradation and water splitting reactions (Khan et al., 2022; Mehtab et al., 2022b; Shanavas et al., 2022). One is the most important and promising development is green synthesis, as it enables the creation of photocatalysts, antibacterial compounds and biofuels (Ali et al., 2021; Mehtab et al., 2022b), in a manner that is non-toxic and environmentally friendly, using water as the solvent and compounds extracted from leaves (Alhalili, 2022). Furthermore, these methods of synthesis require lower pressures and temperatures than traditional synthesis methods (Álvarez-Chimal et al., 2022; Dave et al., 2021).

E-mail address: hbayahia@bu.edu.sa

Peer review under responsibility of King Saud University.



Production and hosting by Elsevier

For example, by using leaf extracts obtained from various plant species, M²⁺Fe₂O₄ nanoparticles can be prepared, where M²⁺ can represent gold (Au), cobalt (Co), nickel (Ni), copper (Cu), or silver (Ag) among other metals (Elumalai et al., 2021; Jaast and Grewal, 2021).

Using zinc to create ZnFe₂O₄ catalysts is attractive, as these nanoparticles are highly magnetic and electrically stable. Furthermore they have biomedical properties, can be prepared using diverse methods and come in a range of sizes, shapes and purities. These qualities lend these materials to be used in a broad range of applications (Din et al., 2020).

To improve the activity of ZnFe₂O₄ photocatalysts, different types of plant extract were used such as *Indigofera tinctoria* (Priya et al., 2020) and *Iresine herbstii* (Dwivedi et al., 2021). The products were calcined at different calcination temperatures, and the increasing of calcination temperatures led to reduce the particle sizes (Balasubramanian and Murali, 2020) and their photodegradation performances of dyes were increased in sunlight. The extracts were acted as both chelating and reducing agents, yielding products with high catalytic activity, pure phases and good crystallinity and size dispersion. The product also showed good voltammetric responses, having a high electrochemical performance, making it a promising material for use in electrochemical applications (Bishnoi et al., 2018).

Drawing upon the research described in (Khan et al., 2015) and (Asimuddin et al., 2020), and building upon our earlier work

<https://doi.org/10.1016/j.jksus.2023.102584>

1018-3647/© 2023 The Author(s). Published by Elsevier B.V. on behalf of King Saud University.

This is an open access article under the CC BY-NC-ND license (<http://creativecommons.org/licenses/by-nc-nd/4.0/>).

(Bayahia, 2022a), ZnFe_2O_4 was prepared and calcined using 500–900 °C. Maximal dye degradation was achieved 600 °C. In the current study, ZnFe_2O_4 that had been calcined at 600 °C was modified using leaf extracts from *Ziziphus mauritiana* and *Salvadora persica*. The materials were characterized and their activities were investigated in the degradation of CV dye. The findings in this work reveal that the performance of these bionanomaterials is more efficient than that of other nanomaterials modified by plant extracts.

2. Experimental

2.1. Materials and methods

All chemicals were of analytical grade and used in the state as purchased, and did not undergo addition or modification. p-Toluenesulfonic acid ($\text{C}_7\text{H}_8\text{O}_3\text{S}\cdot\text{H}_2\text{O}$) was purchased from LOBA CHEMIE PVT.Ltd, whilst $\text{Fe}(\text{NO}_3)_3\cdot 9\text{H}_2\text{O}$, $\text{Zn}(\text{NO}_3)_2\cdot 6\text{H}_2\text{O}$ and NaOH were obtained from Sigma-Aldrich. *Ziziphus mauritiana* and *Salvadora persica* leaves were collected from the Albaha region of Saudi Arabia. The CV dye was purchased from BHD.

2.2. Preparation of *Ziziphus mauritiana* and *Salvadora persica* leaf extracts

Fresh and healthy leaves were rinsed in distilled water then left to dry for 7–10 days at room temperature. Once dry, 10 g of leaves was immersed in 100 mL of 65 °C distilled water and left to infuse for 1 h. The infusion was cooled to room temperature then it was filtered to remove the leaves, which were discarded and used to prepare the ZnFe_2O_4 photocatalysts.

2.3. Preparation of ZnFe_2O_4 using leaf extracts

Appropriate quantities of $\text{Zn}(\text{NO}_3)_2\cdot 6\text{H}_2\text{O}$ and $\text{Fe}(\text{NO}_3)_3\cdot 9\text{H}_2\text{O}$ were weighed out then added to the plant extract solution. The solution was stirred until the temperature reached 65 °C, whereupon 1 g of $\text{C}_7\text{H}_8\text{O}_3\text{S}\cdot\text{H}_2\text{O}$ was added, and stirred continuously for 1 hr; the temperature was kept constant at 65 °C. Coprecipitation was instigated by adding 1 M of NaOH solution in a dropwise manner until pH 12. The precipitate was retrieved, filtered and rinsed in distilled water before rinsing once in ethanol. The solids were dried overnight at 120 °C then annealed at 600 °C for 24 h.

2.4. Characterisation techniques

FT-IR Spectrometry (PerkinElmer Spectrum 100) was conducted using the KBr pellet method, in the range of 400–4000 cm^{-1} . X-ray diffraction analysis was performed using a Bruker D8 advanced powder diffractometer instrument; the diffractometer used $\text{Cu K}\alpha$ radiation ($\lambda = 1.5416 \text{ \AA}$) at the 0.2θ scale, in the range of 10° – 80° , with a scanning step of 0.2° at 45 kV and 40 mV. Scanning electron microscopy (SEM) analysis was conducted using a Hitachi S-4800 device (Tokyo, Japan). Also, a JEOL (JEM-2100F) transmission electron microscope (TEM) was used. A UV-vis spectrophotometer (Philips 8800). The Micromeritics Tristar II 2030 analyzer was used for measuring surface area and porosity.

2.5. Photocatalytic reactions

CV dye solution was using batch reactor at neutral media and under sunlight. 15 mg of photocatalyst was added to 20 mL. The mixture was kept in darkness for 30 min to reach the equilibrium. Then the mixture was exposed to sunlight. Repeated reactions were conducted every-five minutes until all the dye had com-

pletely degraded. Then the separated and clear solution was analysed using UV-vis spectroscopy. Equation (1) was used to calculate the percentage of degradation.

$$\text{Degradation}(\%) = \frac{A_0 - A_t}{A_0} \times 100 \quad (1)$$

where, A_0 is the initial absorbance of dye and A_t is the absorbance of the dye at a different time of the reaction.

3. Results and discussion

3.1. FT-IR analysis

FT-IR was used to identify the functional groups that contributed to the reduction and stabilisation of the synthesized photocatalytic materials (Shanavas et al., 2021; Nasiri et al., 2022). Fig. 1 shows the IR spectra for *Salvadora persica* and *Ziziphus mauritiana* extracts to be in the range of 500–4000 cm^{-1} , it also shows the spectra for the extract-modified ZnFe_2O_4 nanoparticles. The peaks reflect the OH, C–O, CH and C=O functional groups. *Salvadora persica* presents broad peaks of free O–H at 3400, C–H at 2369, the bands at 1632 and 1063 cm^{-1} donate the C=O and C–O respectively and stretching vibrations of C–H at 1439 cm^{-1} (Elumalai et al., 2021).

The spectra of modified ZnFe_2O_4 show peaks that reflect C–H stretch at 2915 cm^{-1} and C=O stretching band at 1632 cm^{-1} . A broad peak at 3440 cm^{-1} is attributed to the stretching vibrations of O–H bonded and $-\text{NH}_2$ functional groups (Cheperli et al., 2022).

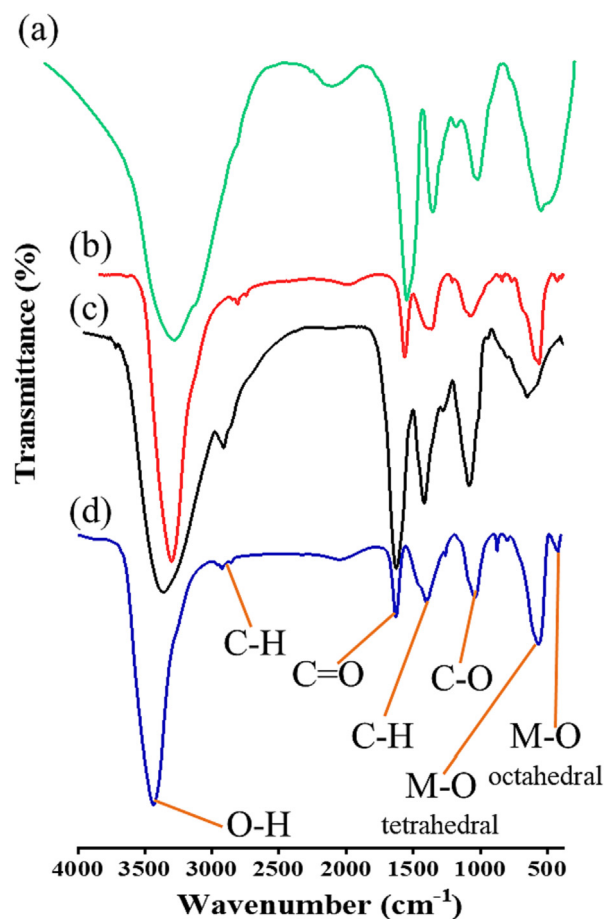


Fig. 1. FT-IR spectra of (a) *Salvadora persica* extract; (b) ZnFe_2O_4 modified by *Salvadora persica* extract; (c) ZnFe_2O_4 modified by *Ziziphus mauritiana* extract; (d) ZnFe_2O_4 modified by *Ziziphus mauritiana* extract.

Meanwhile, the band at $400\text{--}850\text{ cm}^{-1}$ is assigned to M–O stretching vibrations (Din et al., 2020).

These results indicate that the extract contains phytochemicals such as alkaloids, flavonoids, glycosides, tannins and phenolics (Priya et al., 2020). These functional groups are reported cap ZnFe_2O_4 , which facilitates the particles' photocatalytic activity. These functional groups are reported cap ZnFe_2O_4 , which facilitates the particles' photocatalytic activity. These results are consistent with those published elsewhere (Xiu et al., 2022).

3.2. XRD analysis

Fig. 2 presents the XRD results of modified and pure ZnFe_2O_4 photocatalyst. Pure ZnFe_2O_4 has a crystalline structure and sharp XRD peaks and modifying ZnFe_2O_4 with plant extracts reduced the crystallinity of ZnFe_2O_4 . This can be explained by carbon annealing at $600\text{ }^\circ\text{C}$, resulting in an amorphous structure. The

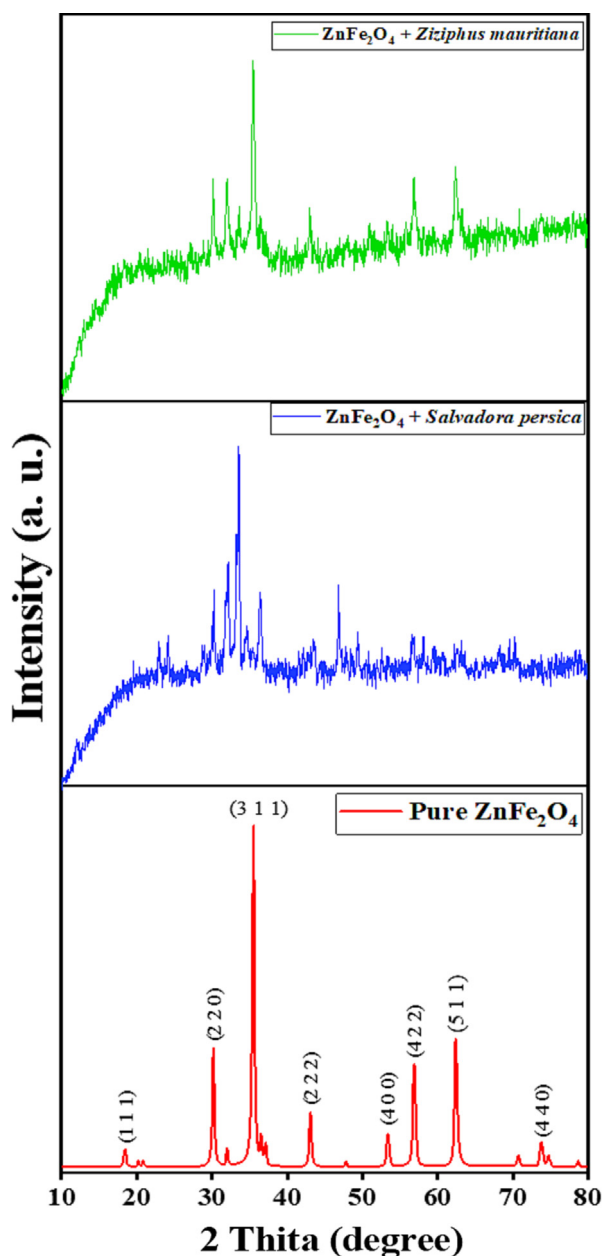


Fig. 2. XRD patterns of pure and modified ZnFe_2O_4 photocatalysts.

diffraction patterns at 30.14 , 35.54 , 36.53 , 43.15 , 53.41 , 56.93 and 62.35 , which are indexed to (220) , (311) , (222) , (400) , (422) , (511) and (440) lattice planes indicate that pure ZnFe_2O_4 nanostructures have a face-centred cubic structure. The assigned diffraction lines are in excellent agreement with corresponding JCPDS No: 00-022-1012 (Bayahia, 2022a). The peaks at 22.91 and 24.09 , which are assigned to Fe_2O_3 impurities that exhibited in the structure of ZnFe_2O_4 treated by *Ziziphus mauritiana* extract. The observed pattern of ZnFe_2O_4 and Fe_2O_3 are consistent with JCPDS cards of # 22-1012 and #87-1166 respectively (Pakzad et al., 2019).

On the basis of the half-width of the 311 reflection in the powder pattern, the average grain size, which was calculated using the Debye-Scherrer formula: $D = 0.9\lambda/\beta \cos \theta$, where D is the crystalline size, λ is the wavelength (1.54), β is the width of the XRD peak posted at 35.54° at half maximum height (FWHM) and θ is the Bragg diffraction angle (Bayahia, 2022b). Table 1 presents the XRD results of the nanoparticles crystalline grain sizes.

3.3. Morphological analysis

3.3.1. SEM and EDS analysis

The results of the SEM analysis of the modified ZnFe_2O_4 are shown in Fig. 3(a) and (b). This reveals that all of samples have broadly spherical morphologies with numerous agglomerations of flakes. Due to the low magnification of the SEM images, it was difficult to obtain measurements of the size of the particles. Treating the ZnFe_2O_4 nanoparticles with different plant extracts yielded products that differed in their morphologies. As Fig. 3(a) demonstrates, treating ZnFe_2O_4 with *Ziziphus mauritiana* extracts produced coarser particles than treating the nanoparticles with *Salvadora persica*, which were finer and more spherical in shape (Fig. 3(b)).

To identify the elemental compositions of the plant-extract modified samples, EDS was used (Fig. 3(c) and (d)). From these images, it can be seen that the samples were pure; the small amount of carbon present was derived from the plant extracts.

The EDS results show that Zn, Fe and O were the only elements present in all of the samples. The plant extracts modified a reasonable percentage of the Zn, Fe and O elements of the ZnFe_2O_4 . The other signals are consistent with the absorption of carbon, confirming the presence of plant extract-derived organic compounds, which act as capping ligands for the photocatalysts. The EDS results presented in Fig. 3(c) and (d) are aligned with others reported elsewhere (Gupta et al., 2020).

3.3.2. TEM analysis

The particle sizes of both pure and modified ZnFe_2O_4 NPs were measured using TEM (Fig. 4(a) and (b)). The sizes of modified and unmodified photocatalyst were 7.59 nm and 5.95 nm for Pure ZnFe_2O_4 , ZnFe_2O_4 by *Ziziphus mauritiana* and ZnFe_2O_4 by *Salvadora persica* respectively. The morphologies of the nanoparticles in the images are spherical, indicative of organic compounds being present, which would have come from the plant extracts.

The results show that the agglomerations of NPs were excessed in all of the samples. This confirms that the residual organic compounds from the plant extracts were acting as capping ligands for the ZnFe_2O_4 photocatalysts. Using plant extracts reduced the amount of agglomeration. Using *Salvadora persica* extract resulted in small diameter particle sizes, which was expected when the capping method was used for ZnFe_2O_4 synthesis.

Fig. 4(c) and (d) present the results of the selected area electron diffraction (SAED) pattern. The SAED patterns reveal that the prepared materials are polycrystalline structures (Balasubramanian and Murali, 2020). The rings correspond to the crystal planes of

Table 1
Data of crystallite, average particle size and band gap.

Sample	Position of highest peak (deg.)	Crystalline Size (nm)	Average particle size (nm)	Optical Band Gap energy (eV)
ZnFe ₂ O ₄ <i>Ziziphus mauritiana</i>	35.49	18.39	7.59	1.37–2.12
ZnFe ₂ O ₄ <i>Salvadora persica</i>	33.59	17.30	5.95	1.43–1.82

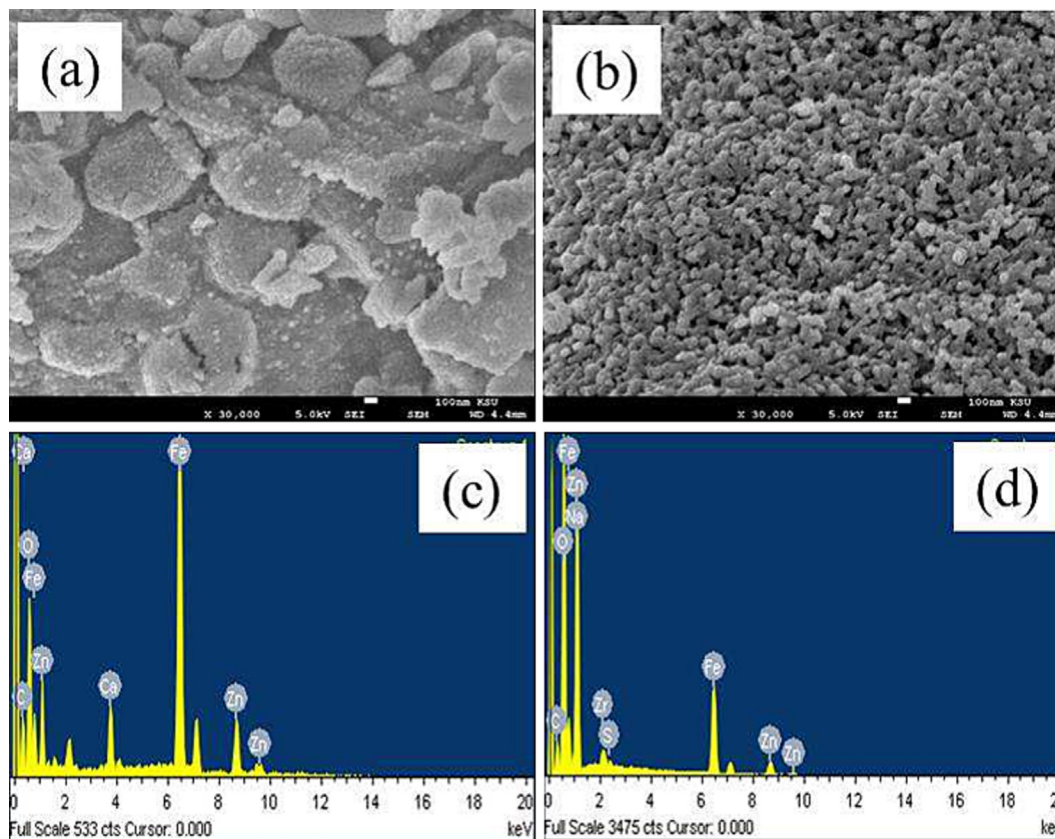


Fig. 3. SEM images of ZnFe₂O₄ modified with (a) *Ziziphus mauritiana* (b) *Salvadora persica*; and EDS images of ZnFe₂O₄ modified with (c) by *Ziziphus mauritiana* (d) *Salvadora persica*.

(220), (311), (400) (511) and (440). As confirmed by analysing the XRD patterns, the prepared nanoparticles were crystalline.

The histograms plots shown in Fig. 4(e) and (f) depict the distribution of the size of the particles created, which was determined by analysing TEM images (Asimuddin et al., 2020). Comparing the two histograms shows that the distribution of ZnFe₂O₄ modified with *Ziziphus mauritiana* is narrower in scope than that of ZnFe₂O₄ modified with *Salvadora persica*. The difference in the distribution of particle sizes might play a role in photodegradation performance.

3.4. Optical properties analysis

Fig. 5(a) shows that, the prepared materials absorbed light radiation in the range of 480–850 nm, indicating they were active in sunlight. To calculate the band-gap energy the following equation was used: E_g (eV) = $1240/\lambda$ (Bayahia, 2022b), where, E_g is the band gap energy, and λ is the incident light wavelength (nm).

Based on the results in Fig. 5(a), Tauc plots were used to estimate the value of band gap energies of the ZnFe₂O₄ modified nanoparticles. The following equation was used: $(Ah\nu)^n = B(h\nu - E_g)$ where, A is the light absorbance, $h\nu$ is the photon energy, B is the constant related, and n can be $\frac{1}{2}$ or 2 for direct or indirect transitions, respectively. Table 1 and Fig. 5(b and c) show that

the band gaps for ZnFe₂O₄ modified with plant extracts are lower than the band gaps for pure ZnFe₂O₄ (Bayahia, 2022a). The band gaps were affected by doping ZnO with Fe; the capping activity of the plant extracts might have reduced the band gap values and Fermi level was achieved due to the excitation of electrons was from valance band (VB) to conduction band (CB).

3.5. Textural properties

The specific BET surface areas, pore volumes and pore diameters of the modified ZnFe₂O₄ nanoparticles are presented in Table 2. The different extracts resulted in ZnFe₂O₄ adopting different textural properties. Using the *Salvadora persica* extract gave the nanoparticles a significantly larger surface area than using the *Ziziphus mauritiana* extract. Fig. 6 shows that the modified photocatalysts presented as mesoporous structures. The prepared biomaterials in this study are matched the fact of materials with greater surface area and pore volume have great numbers of active site located on the surfaces (Algarni et al., 2022).

3.6. Photocatalytic dye degradation studies

In our previous study (Bayahia, 2022a), the ability of ZnFe₂O₄ nanoparticles to degrade CV dye in solution was compared against

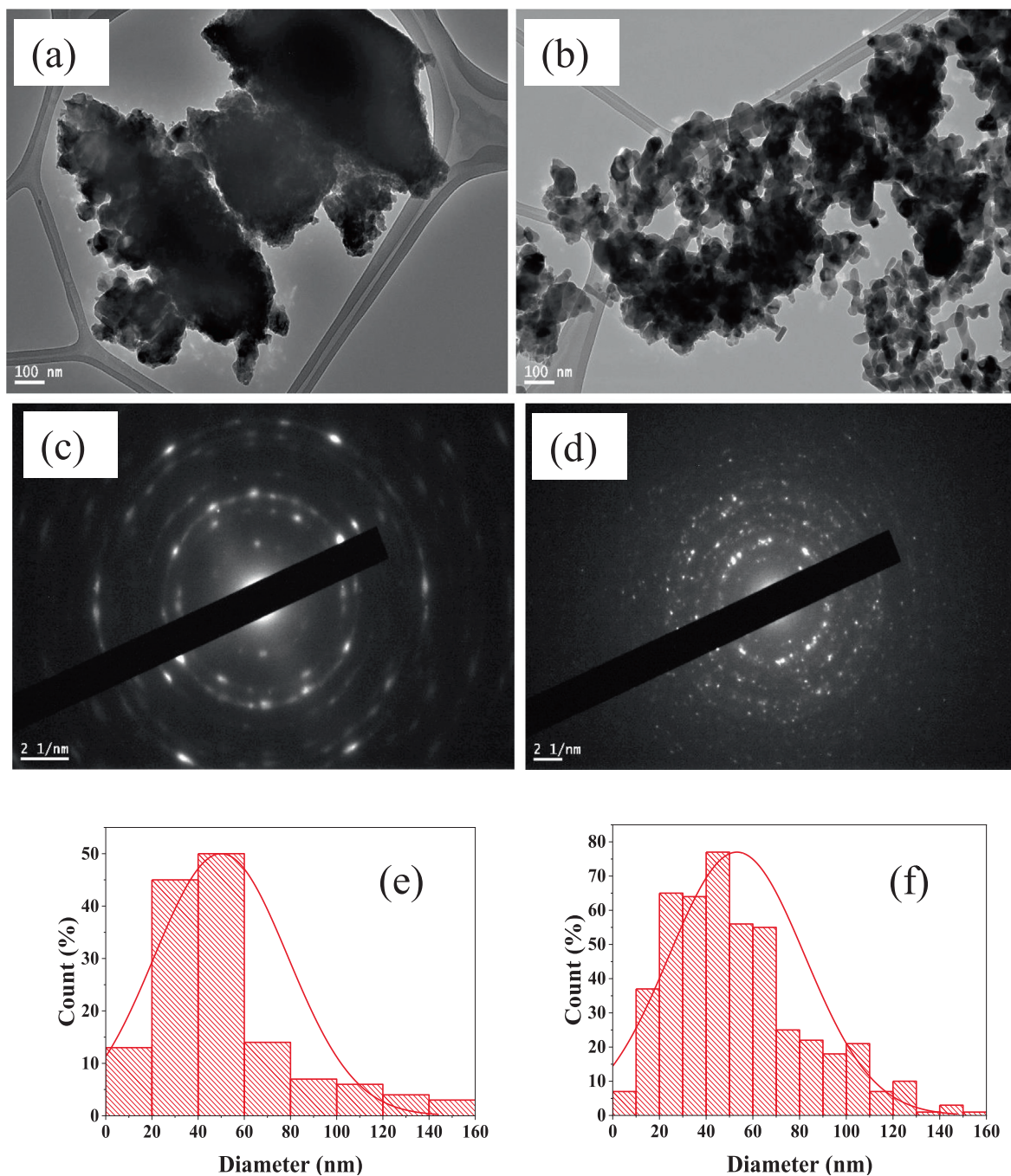


Fig. 4. TEM images of ZnFe₂O₄ modified with (a) *Ziziphus mauritiana* (b) *Salvadora persica*. SAED images of ZnFe₂O₄ modified with (c) *Ziziphus mauritiana* (d) *Salvadora persica*. Distribution of different particle sizes for ZnFe₂O₄ modified by (e) *Ziziphus mauritiana* (f) *Salvadora persica*.

the abilities of CuFe₂O₄, CoFe₂O₄ and NiFe₂O₄ nanoparticles. The photocatalysts were prepared using the co-precipitation method; these were then calcined at temperatures ranging between 500 °C and 900 °C. Maximum catalytic performance was achieved when catalysts were calcined at 600 °C. Consequently, for this study, ZnFe₂O₄ was selected for modification with *Salvadora persica* and *Ziziphus mauritiana* extracts, and calcined at 600 °C.

The ability of ZnFe₂O₄ treated with to photodegrade CV dye under the visible light conditions was explored. The different plant extracts exhibited different degradative abilities. The plant extracts affected the photocatalytic activity of the nanoparticles. In this instance, treating ZnFe₂O₄ with *Ziziphus mauritiana* resulted in poorer elimination of CV dye compared to ZnFe₂O₄ treated with

Salvadora persica; the reaction and sunlight conditions were consistent for both samples.

Fig. 7(a) and (b) shows the dark and in sunlight conditions using 10 ppm of CV dye solutions. No dye was degraded in the blank condition, but there was some degradation of dye in the darkness condition. The results are similar to those described previously (Algarni et al., 2022).

For the comparative photocatalytic activity, 15 mg of modified ZnFe₂O₄ was used under the sunlight conditions. The photocatalytic activities of the modified ZnFe₂O₄ photocatalysts were improved by using neutral pH and sunlight (Fig. 7c-f). Two concentrations of CV dye (10 and 30 ppm) were loaded with 15 mg of plant extract-modified ZnFe₂O₄ nanoparticles. ZnFe₂O₄ with

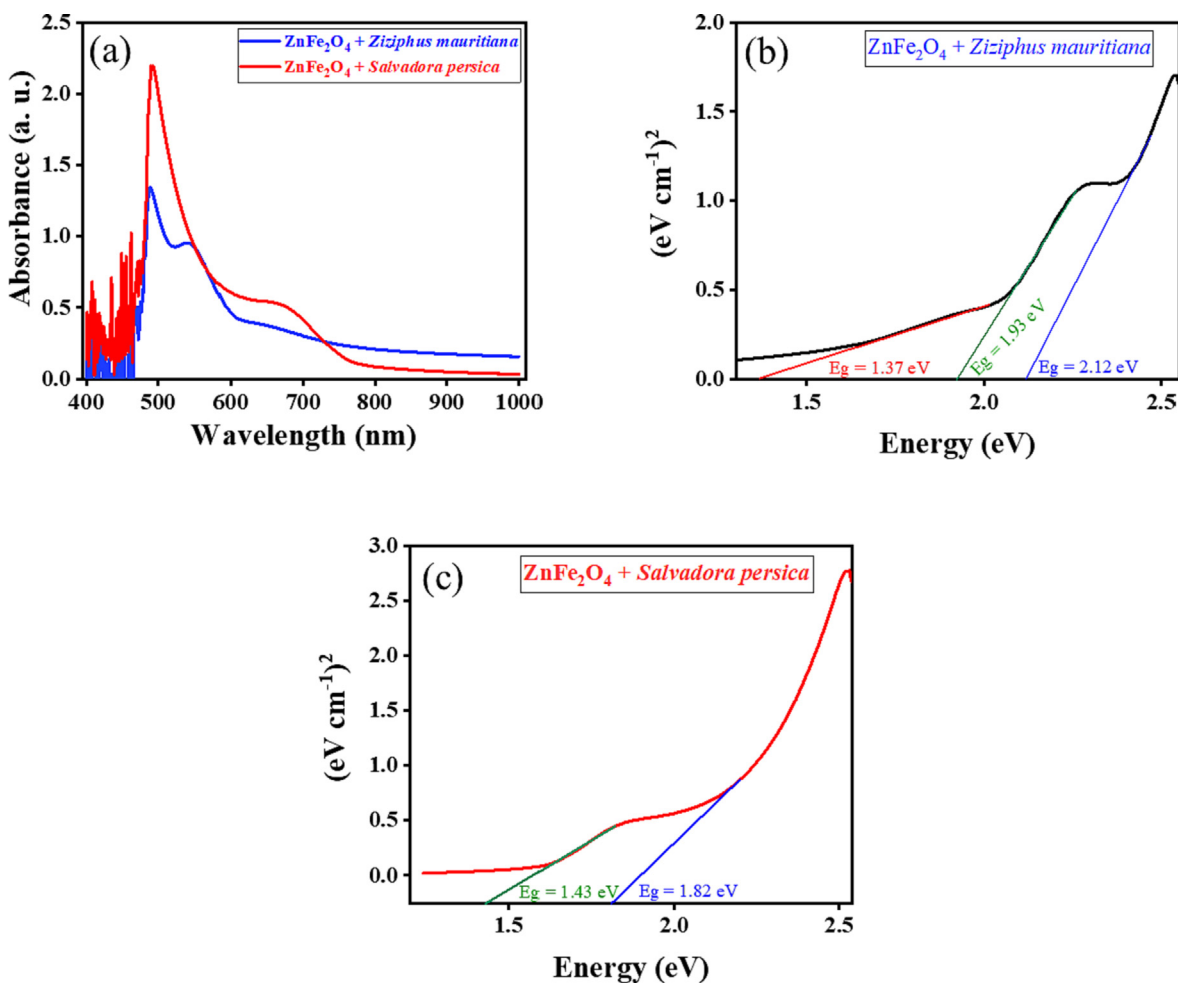


Fig. 5. UV-vis absorption spectra (a) and plots of $(Ah\nu)^n$ as a function of photon energy ($h\nu$) of $ZnFe_2O_4$ treated by plant extracts (b, c).

Table 2

Textural properties and kinetic studies of $ZnFe_2O_4$ for the photodegradation of CV solutions.

Photocatalysts	BET surface area (m^2/g)	Pore Volume (cm^3/g)	Pore Size (\AA)	[CV] (ppm)	Degradation time (min)	k_{app} (min^{-1})	$t_{1/2}$ (min)
$ZnFe_2O_4 + Salvadoria persica$	3.583	0.0317	533.53	10	12	0.65	1.07
				30	25	0.16	4.33
$ZnFe_2O_4 + Ziziphus mauritiana$	0.965	0.0079	570.55	10	19	0.13	5.33
				30	30	0.10	6.93

Salvadora persica extract achieved maximum photocatalytic degradation of 10 ppm of CV dye in 12 min (Fig. 7c). For pure $ZnFe_2O_4$, the maximum photocatalytic degradation of dye was reached in 30 min (Fig. 7d). This is consistent with earlier studies reported in the literature (Bayahia, 2022a).

The photodegradative ability of *Salvadora persica* modified photocatalysts declined when the concentration of CV rose to 30 ppm. It reached maximum photodegradation within 25 min, which is longer than when the concentration of dye was 10 ppm. However, the performance of *Salvadora persica* modified photocatalysts was superior to the catalysts modified with *Ziziphus mauritiana* at the same concentration and exposed to the same conditions (Fig. 7 (e) and (f)).

Several factors influence the photocatalytic degradation of dye in solution, including the duration of exposure, the concentration of the dye and the intensity of the sunlight (Oliveira et al., 2020).

This work shows that the type of plant extract used to modify the photocatalysts is also influential. Compared to $ZnFe_2O_4$ modified with *Ziziphus mauritiana*, samples treated with *Salvadora persica* were more effective at degrading the dye. The plant extracts have several qualities, acting as stabilisers, reducing agents and the caps for the metals (Lau et al., 2020).

3.7. Kinetics studies

This study explored the photocatalytic rate of $ZnFe_2O_4$ modified with plant extract exposed to different concentrations of CV dye. The reactions followed pseudo-first-order kinetics and the initial decomposition reaction was calculated using the pseudo-first-order kinetic law (Lau et al., 2020).

$$-\ln C/C_0 = k_{app}t$$

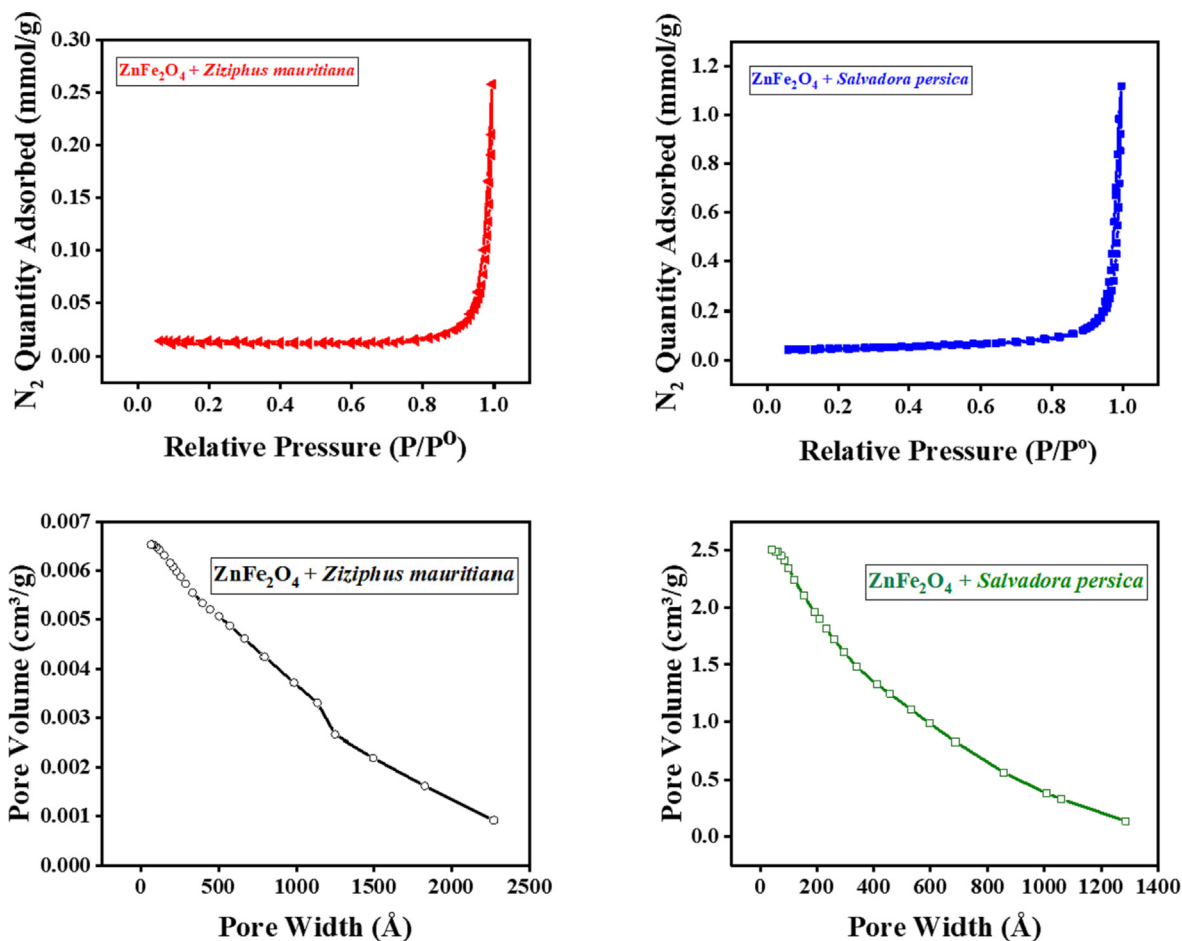


Fig. 6. BET results of ZnFe₂O₄ modified by plant extracts.

where k_{app} is the rate constant of the pseudo-first-order reaction and t is the reaction time.

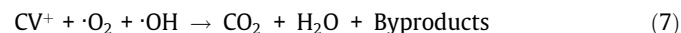
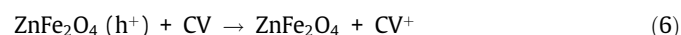
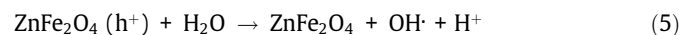
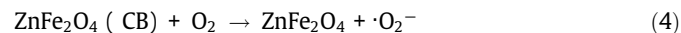
Table 2 presents the half-life and rate constant results. Compared to unmodified ZnFe₂O₄, modified nanoparticles displayed greater photodegradative ability, which is attributed to their morphological, structural and textural properties. Photocatalysts with high crystallite sizes and small particle sizes have fewer surfaced defects, which typically acts as recombination centres for the electron-hole pairs.

The dye concentration significantly affected the photocatalytic degradation undertaken by the nanoparticles. Modified photocatalysts were able to degrade dye concentrations of 10 and 30 ppm in less time than unmodified photocatalysts. ZnFe₂O₄ modified by *Salvadora persica* has smaller particle size with lower band gap and higher performance of photocatalytic degradation than ZnFe₂O₄ modified by *Ziziphus mauritiana*. Materials with smaller particle sizes have lower band gap and the decreasing of band gap can be increased the oxygen vacancy and the energy level (Deotale and Nandedkar, 2016), which can be decreased recombination of \bar{e} and h^+ (Yang et al., 2022). The results of C/C_0 vs time and $\ln C/C_0$ vs time plots are presented in Fig. 7(α - ϵ).

3.8. Mechanism of photocatalytic degradation of CV dye

The proposed mechanisms by which modified ZnFe₂O₄ nanoparticles photocatalytically degrades CV dye are as follows. First, CV dye adsorbs to the surface of the ZnFe₂O₄ photocatalysts. When exposed to sunlight, the electrons (\bar{e}) in VB gets excited to the CB and hole ions (h^+) was generate in the VB of the photocat-

alysts. Oxygen was reduced by electrons in the CB to become superoxide radicals ($\cdot O_2$) (Álvarez-Chimal et al., 2022; Dwivedi et al., 2021). The h^+ attack the water molecules, releasing hydroxyl radicals ($\cdot OH$). Radicals were attacked CV dye and degraded into CO₂ and H₂O (Rahmayeni et al., 2021) as equations (3)–(7) and Fig. 8 (left) show.



3.9. Reusability test

To evaluate the reusability of the ZnFe₂O₄ photocatalysts created in this study, five iterations of recycling experiments were conducted under the same conditions. Fig. 8 (right) shows the decline in degradative ability of one set of photocatalysts after each cycle of use. After completing a reaction, the photocatalysts were retrieved, rinsed in distilled water and acetone, dried overnight in an oven set at 120° C and tested at the same conditions of fresh one. With each iteration, the photocatalytic degradation of CV dye declined, falling from 91 % in the first cycle, to 85 % in the fifth

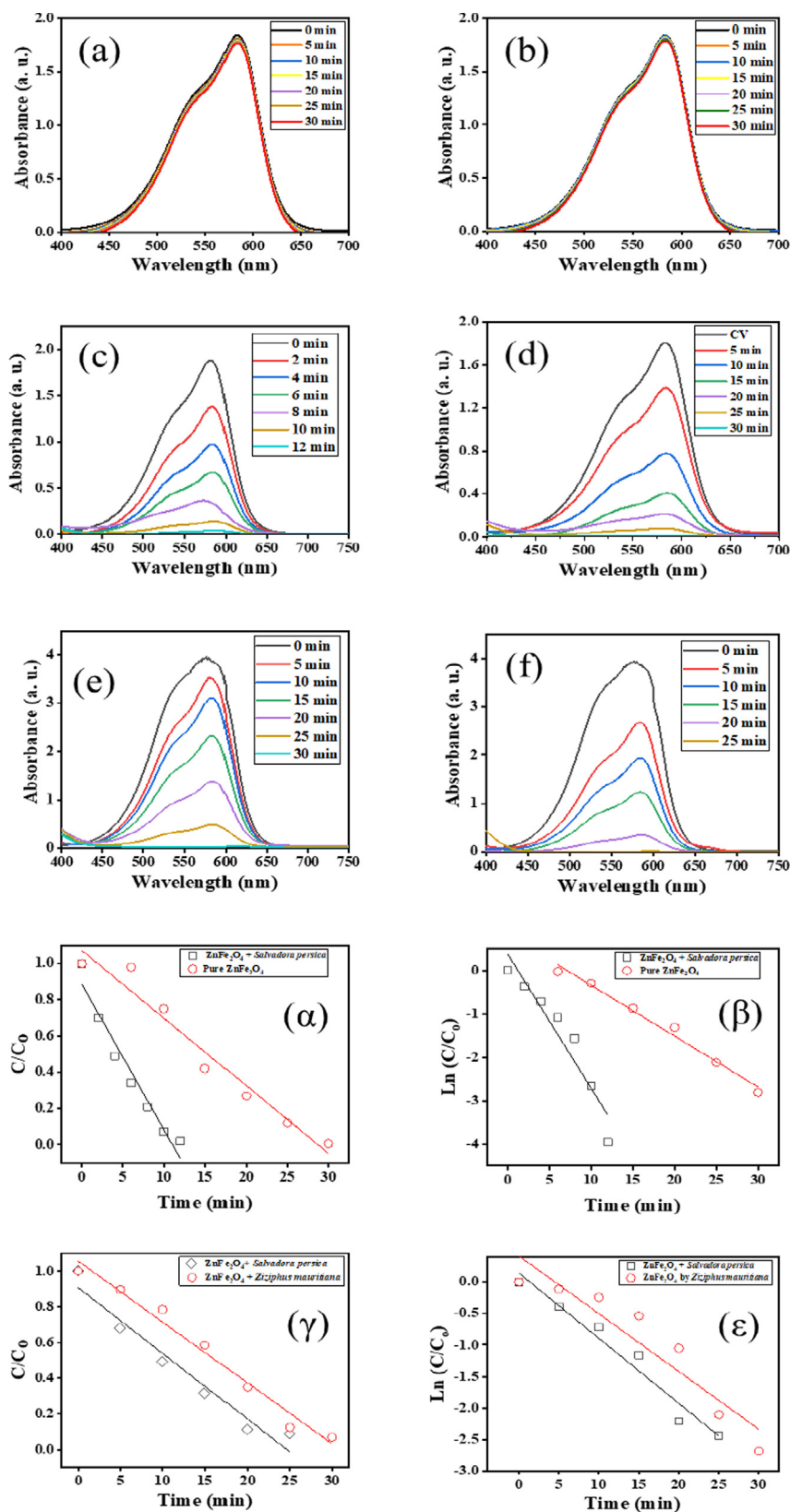


Fig. 7. UV–vis spectra of photocatalytic degradation of (a) catalysts in darkness (b) blank (no catalyst) (c) *Salvadoria persica*-modified $ZnFe_2O_4$ in 10 ppm CV (d) Pure $ZnFe_2O_4$ in 10 ppm CV (e) *Ziziphus mauritiana*-modified $ZnFe_2O_4$ in 30 ppm CV dye (f) *Salvadoria persica*-modified $ZnFe_2O_4$ in 30 ppm CV and C/C_0 vs time (α , γ) and $\ln(C/C_0)$ vs time (β , ϵ) for pure and modified $ZnFe_2O_4$ with a CV dye concentration of 10 ppm (top) and 30 ppm (bottom).

cycle. This small decline reflects changes to the morphological, optical and textural properties of the photocatalysts. The results

of the reusability experiments are similar to those reported by other researchers (Rahmayeni et al., 2021; Malik et al., 2022).

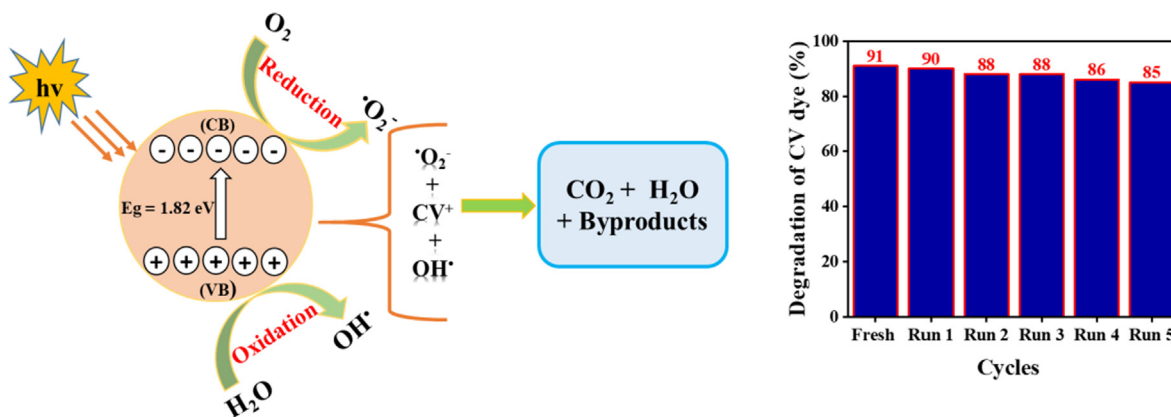


Fig. 8. Schematic diagram of the photocatalytic degradation of CV solution (left) and percentage of decline in photodegradation of 30 ppm of CV dye exposed to recovered $ZnFe_2O_4$ photocatalysts modified with *Salvadora persica* extract (right).

4. Conclusions

This study shows that modifying $ZnFe_2O_4$ nanoparticles with *Salvadora persica* and *Ziziphus mauritiana* extracts creates nanoparticle products with superior ability to photodegrade CV dye solution in sunlight. The method used to synthesise the materials, their morphological, optical and textural properties and the reaction duration significantly influences the surface structure, optical properties, particle size and particle size distributions of $ZnFe_2O_4$ treated with *Salvadora persica*. The photocatalyst was stable, being able to be used five times without experiencing marked decline in photocatalytic performance.

Declaration of Competing Interest

The authors declare that they have no known competing financial interests or personal relationships that could have appeared to influence the work reported in this paper.

Acknowledgment

The author would like to thank the Deanship of Scientific Research, Albaha University, Saudi Arabia for the project fund (1442/29).

Appendix A. Supplementary material

Supplementary data to this article can be found online at <https://doi.org/10.1016/j.jksus.2023.102584>.

References

- Algarni, T., Abduh, N. A. Y., al Kahtani, A., & Aouissi, A. (2022). Photocatalytic degradation of some dyes under solar light irradiation using ZnO nanoparticles synthesized from *Rosmarinus officinalis* extract. In: *Green Chemistry Letters and Reviews*, vol. 15, issue 2, Taylor and Francis Ltd. pp. 460–473, <https://doi.org/10.1080/17518253.2022.2089059>.
- Alhalili, Z. (2022). Green synthesis of copper oxide nanoparticles CuO NPs from *Eucalyptus Globoulus* leaf extract: Adsorption and design of experiments. *Arab. J. Chem.* 15 (5). <https://doi.org/10.1016/j.arabjc.2022.103739>.
- Ali, S.S., Al-Tohamy, R., Koutra, E., Kornaros, M., Khalil, M., Elsamahy, T., El-Shetehy, M., Sun, J., 2021. Coupling azo dye degradation and biodiesel production by manganese-dependent peroxidase producing oleaginous yeasts isolated from wood-feeding termite gut symbionts. *Biotechnol. Biofuels* 14 (1). <https://doi.org/10.1186/s13068-021-01906-0>.
- Álvarez-Chimal, R., García-Pérez, V.I., Álvarez-Pérez, M.A., Tavera-Hernández, R., Reyes-Carmona, L., Martínez-Hernández, M., Arenas-Alatorre, J.Á., 2022. Influence of the particle size on the antibacterial activity of green synthesized zinc oxide nanoparticles using *Dysphania ambrosioides* extract, supported by molecular docking analysis. *Arab. J. Chem.* 15, (6). <https://doi.org/10.1016/j.arabjc.2022.103804>.
- Asimuddin, M., Shaik, M.R., Fathima, N., Afreeen, M.S., Adil, S.F., Siddiqui, M.R.H., Jamil, K., Khan, M., 2020. Study of antibacterial properties of ziziphus mauritiana based green synthesized silver nanoparticles against various bacterial strains. *Sustainability (Switzerland)* 12 (4). <https://doi.org/10.3390/su12041484>.
- Balasubramanian, M., Murali, K.R., 2020. Biosynthesis of zinc ferrite ($ZnFe_2O_4$) nanoparticles using flower extract of *nyctanthes arbor-tristis* and their photocatalytic activity. *Ferroelectrics* 555 (1), 1–14. <https://doi.org/10.1080/00150193.2019.1691381>.
- Bayahia, H., 2022a. High activity of $ZnFe_2O_4$ nanoparticles for photodegradation of crystal violet dye solution in the presence of sunlight. *J. Taibah Univ. Sci.* 16 (1), 988–1004. <https://doi.org/10.1080/16583655.2022.2134696>.
- Bayahia, H., 2022b. Green synthesis of activated carbon doped tungsten trioxide photocatalysts using leaf of basil (*Ocimum basilicum*) for photocatalytic degradation of methylene blue under sunlight. *J. Saudi Chem. Soc.* 26 (2). <https://doi.org/10.1016/j.jscs.2022.101432>.
- Bishnoi, S., Kumar, A., Selvaraj, R., 2018. Facile synthesis of magnetic iron oxide nanoparticles using inedible *Cynometra ramiflora* fruit extract waste and their photocatalytic degradation of methylene blue dye. *Mater. Res. Bull.* 97, 121–127. <https://doi.org/10.1016/j.materresbull.2017.08.040>.
- Cheperli, A.-M., Mokaber-Esfahani, M., Farhad, A.T., 2022. Biosynthesis, characterization and antimicrobial activities of zinc oxide nanoparticles from leaf & seed extracts of *Malva neglecta* Wallr. <https://doi.org/10.21203/rs.3.rs-1286975/v1>.
- Dave, S., Khan, A.M., Purohit, S.D., Suthar, D.L., 2021. Application of Green Synthesized Metal Nanoparticles in the Photocatalytic Degradation of Dyes and Its Mathematical Modelling Using the Caputo-Fabrizio Fractional Derivative without the Singular Kernel. *J. Math. (Wuhan)* 2021. <https://doi.org/10.1155/2021/9948422>.
- Deotale, A.J., Nandedkar, R.V., 2016. Correlation between particle size, strain and band gap of iron oxide nanoparticles. *Mater. Today: Proc.* 3 (6), 2069–2076. <https://doi.org/10.1016/j.matpr.2016.04.110>.
- Din, M.I., Jabbar, S., Najeeb, J., Khalid, R., Ghaffar, T., Arshad, M., Khan, S.A., Ali, S., 2020. Green synthesis of zinc ferrite nanoparticles for photocatalysis of methylene blue. *Int. J. Phytorem.* 22 (13), 1440–1447. <https://doi.org/10.1080/15226514.2020.1781783>.
- Dwivedi, P., Jatrana, I., Khan, A.U., Khan, A.A., Satiya, H., Khan, M., Moon, I.S., Alam, M., 2021. Photoremediation of methylene blue by biosynthesized ZnO/Fe_2O_4 nanocomposites using *Callistemon viminalis* leaves aqueous extract: A comparative study. *Nanotechnol. Rev.* 10 (1), 1912–1925. <https://doi.org/10.1515/ntrev-2021-0117>.
- Elumalai, N., Prabhu, S., Selvaraj, M., Shanavas, S., Navaneethan, M., Harish, S., Ramu, P., Ramesh, R., 2021. Investigation on synergistic effect of rGO and carbon quantum dots-embedded ZnO hollow spheres for improved photocatalytic aqueous pollutant removal process. *J. Mater. Sci. Mater. Electron.* 32 (24), 28633–28647. <https://doi.org/10.1007/s10854-021-07239-w>.
- Gupta, N.K., Ghaffari, Y., Kim, S., Bae, J., Kim, K.S., Saifuddin, M., 2020. Photocatalytic degradation of organic pollutants over MFe_2O_4 ($M = Co, Ni, Cu, Zn$) nanoparticles at neutral pH. *Sci. Rep.* 10(1), 1–0. <https://doi.org/10.1038/s41598-020-61930-2>.
- Haseena, S., Jayamani, N., Shanavas, S., Duraimurugan, J., Haija, M.A., Kumar, G.S., Kumar, A.S., Prabhuraj, T., Maadeswaran, P., Acevedo, R., 2022. Bio-synthesis of photocatalytic Fe_2O_3 nanoparticles using *Leucas aspera* and *Jatropha podagrica* leaf extract for an effective removal of textile dye pollutants. *Optik* 249. <https://doi.org/10.1016/j.ijleo.2021.168275>.
- Jaast, S., Grewal, A., 2021. Green synthesis of silver nanoparticles, characterization and evaluation of their photocatalytic dye degradation activity. *Curr. Res. Green Sustainable Chem.* 4. <https://doi.org/10.1016/j.crgsc.2021.100195>.
- Khan, M., Al-Marri, A.H., Khan, M., Shaik, M.R., Mohri, N., Adil, S.F., Kuniyil, M., Alkhatlan, H.Z., Al-Warthan, A., Tremel, W., Tahir, M.N., Siddiqui, M.R.H., 2015.

- Green approach for the effective reduction of graphene oxide using *Salvadora persica* L. root (Miswak) extract. *Nanoscale Res. Lett.* 10 (1), 1–9. <https://doi.org/10.1186/s11671-015-0987-z>.
- Khan, H., Lone, I.H., Lofland, S.E., Ramanujachary, K.V., Ahmad, T., 2022. Exploiting multiferroicity of TbFeO_3 nanoparticles for hydrogen generation through photo/electro/photoelectro-catalytic water splitting. *Int. J. Hydrogen Energy*. <https://doi.org/10.1016/j.ijhydene.2022.11.143>.
- Lau, G.E., Abdullah, C.A.C., Ahmad, W.A.N.W., Assaw, S., Zheng, A.L.T., 2020. Eco-friendly photocatalysts for degradation of dyes. *Catalysts* 10 (10), 1–16. <https://doi.org/10.3390/catal10101129>.
- Malik, A.R., Sharif, S., Shaheen, F., Khalid, M., Iqbal, Y., Faisal, A., Aziz, M.H., Atif, M., Ahmad, S., Fakhar-e-Alam, M., Hossain, N., Ahmad, H., Botmart, T., 2022. Green synthesis of RGO-ZnO mediated *Ocimum basilicum* leaves extract nanocomposite for antioxidant, antibacterial, antidiabetic and photocatalytic activity. *J. Saudi Chem. Soc.* 26 (2). <https://doi.org/10.1016/j.jscs.2022.101438>.
- Mehtab, A., Ahmed, J., Alshehri, S.M., Mao, Y., Ahmad, T., 2022a. Rare earth doped metal oxide nanoparticles for photocatalysis: A perspective. In: *Nanotechnology*, vol. 33, Issue 14, IOP Publishing Ltd. <https://doi.org/10.1088/1361-6528/ac43e7>.
- Mehtab, A., Banerjee, S., Mao, Y., Ahmad, T., 2022b. Type-II CuFe_2O_4 /Graphitic Carbon Nitride Heterojunctions for High-Efficiency Photocatalytic and Electrocatalytic Hydrogen Generation. *ACS Appl. Mater. Interfaces* 14 (39), 44317–44329. <https://doi.org/10.1021/acsami.2c11140>.
- Nasiri, A., Rajabi, S., Hashemi, M., 2022. CoFe_2O_4 @Methylcellulose/AC as a New, Green, and Eco-friendly Nano-magnetic adsorbent for removal of Reactive Red 198 from aqueous solution. *Arab. J. Chem.* 15 (5). <https://doi.org/10.1016/j.arabjc.2022.103745>.
- Oliveira, T.P., Marques, G.N., Macedo Castro, M.A., Viana Costa, R.C., Rangel, J.H.G., Rodrigues, S.F., dos Santos, C.C., Oliveira, M.M., 2020. Synthesis and photocatalytic investigation of ZnFe_2O_4 in the degradation of organic dyes under visible light. *J. Mater. Res. Technol.* 9 (6), 15001–15015. <https://doi.org/10.1016/j.jmrt.2020.10.080>.
- Pakzad, K., Alinezhad, H., Nasrollahzadeh, M., 2019. Green synthesis of $\text{Ni@Fe}_3\text{O}_4$ and CuO nanoparticles using *Euphorbia maculata* extract as photocatalysts for the degradation of organic pollutants under UV-irradiation. *Ceram. Int.* 45 (14), 17173–17182. <https://doi.org/10.1016/j.ceramint.2019.05.272>.
- Priya, D.D., Roopan, S.M., Singh, S., Bansal, J., Shanavas, S., Khan, M.R., Al-Dhabi, N.A., Arasu, M.V., Durairamdiyan, V., 2020. Phyto-synthesis of CuO nano-particles and its catalytic application in C-S bond formation. *Mater. Lett.* 266. <https://doi.org/10.1016/j.matlet.2020.127486>.
- Rahmayeni, Febrialita, R., Stiadi, Y., Putri, Y.E., Sofyan, N., Zulhadjri, 2021. Simbang Darah (Iresine herbstii) extract mediated hydrothermal method in the synthesis of zinc ferrite spinel nanoparticles used for photocatalysis and antibacterial applications. *J. Environ. Chem. Eng.* 9(2). <https://doi.org/10.1016/j.jece.2021.105140>.
- Shanavas, S., Ahamad, T., Alshehri, S.M., Acevedo, R., Anbarasan, P.M., 2021. A facile microwave route for fabrication of NiO/rGO hybrid sensor with efficient CO_2 and acetone gas sensing performance using clad modified fiber optic method. *Optik* 226. <https://doi.org/10.1016/j.ijleo.2020.165970>.
- Shanavas, S., Haija, M.A., Singh, D.P., Ahamad, T., Roopan, S.M., van Le, Q., Acevedo, R., Anbarasan, P.M., 2022. Development of high efficient $\text{Co}_3\text{O}_4/\text{Bi}_2\text{O}_3/\text{rGO}$ nanocomposite for an effective photocatalytic degradation of pharmaceutical molecules with improved interfacial charge transfer. *J. Environ. Chem. Eng.* 10 (2). <https://doi.org/10.1016/j.jece.2022.107243>.
- Xiu, J., Zhang, Y., Paray, B.A., Gulnaz, A., War, M.U.D., 2022. Facile preparation of Fe_2O_3 nanoparticles mediated by *Centaurea alba* extract and assessment of the anti-atherosclerotic properties. *Arab. J. Chem.* 15 (1). <https://doi.org/10.1016/j.arabjc.2021.103493>.
- Yang, Y., Zhao, S., Bi, F., Chen, J., Li, Y., Cui, L., Xu, J., Zhang, X., 2022. Oxygen-vacancy-induced O_2 activation and electron-hole migration enhance photothermal catalytic toluene oxidation. *Cell Reports Phys. Sci.* 3 (8). <https://doi.org/10.1016/j.xcrp.2022.101011>.